

# Exact Fisher zeros and thermofield dynamics across a quantum critical point

Yang Liu,<sup>1</sup> Songtai Lv,<sup>1</sup> Yuchen Meng,<sup>1</sup> Zefan Tan,<sup>1</sup> Erhai Zhao,<sup>2,\*</sup> and Haiyuan Zou<sup>1,†</sup>

<sup>1</sup>Key Laboratory of Polar Materials and Devices (MOE),

School of Physics and Electronic Science, East China Normal University, Shanghai 200241, China

<sup>2</sup>Department of Physics and Astronomy, George Mason University, Fairfax, Virginia 22030, USA

By setting the inverse temperature  $\beta$  loose to occupy the complex plane, Michael E. Fisher showed that the zeros of the complex partition function  $Z$ , if approaching the real  $\beta$  axis, reveal a thermodynamic phase transition. More recently, Fisher zeros have been used to mark the dynamical phase transition in quench dynamics. The success of Fisher zeros however seems limited, and it is unclear how they can be employed to shed light on quantum phase transitions or the non-unitary dynamics of open quantum systems. Here we answer this question by a comprehensive analysis of the (analytically continued) one-dimensional transverse field Ising model. We exhaust all the Fisher zeros to show that in the thermodynamic limit they congregate into a remarkably simple pattern in the form of continuous open or closed lines. These Fisher lines evolve smoothly as the coupling constant is tuned, and a qualitative change identifies the quantum critical point. By exploiting the connection between  $Z$  and the thermofield double states, we obtain analytical expressions for the short- and long-time dynamics of the survival amplitude and the scaling of recurrence time at the quantum critical point. We further point out  $Z$  can be realized and probed in monitored quantum circuits. The analytical results are corroborated by numerical tensor renormalization group which elevates the approach outlined here to a powerful tool for interacting quantum systems.

There is a renewed interest in the concept of complex-valued partition function and its zeros in quantum many-body physics. In the seminal work of Lee and Yang on phase transitions, the magnetic field in spin Hamiltonians (or the chemical potential in a grand canonical ensemble) is analytically continued to take on complex values [1, 2]. Then phase transitions in the thermodynamic limit can be inferred and analyzed by tracking the zeros of the complex-valued partition function  $Z$  evaluated for finite-size systems. Fisher extended the recipe by allowing the inverse temperature  $\beta = 1/k_B T$  to be complex instead, which applies to all systems [3]. Yet, compared to the Lee-Yang zeros, the Fisher zeros are more challenging to find or analyze. Because  $\beta$  couples to every term in the Hamiltonian, the locations of Fisher zeros on the complex  $\beta$  plane appear to feature less regularity. They may not form simple smooth curves as the thermodynamic limit is approached, in sharp contrast to the celebrated circle theorem for Lee-Yang zeros [1, 2]. Such ostensible complexity may be responsible for the scarcity of exact results on Fisher zeros (for a review, see Ref. [4]).

Fisher zeros were invented to comprehend thermodynamic phase transitions. Recently, several of us [5] proposed to use them to probe quantum phase transitions [6]. Numerical data on the one-dimensional transverse field Ising Model (1DTFIM) reveal that as the coupling constant (the transverse field)  $g$  is tuned, the motion of certain Fisher zeros correlates with the energy gap associated with the domain wall excitations. The analysis of Ref. [5] was limited to  $g \leq 1$ , so a natural question is what happens on the disordered side  $g > 1$ . Naively, one might expect from the Kramers-Wannier (KW) duality [7] that the zeros at  $g > 1$  simply mirror those at  $g < 1$ . This conjecture turns out to be false. We shall show that the KW duality breaks down for complex  $\beta$ .

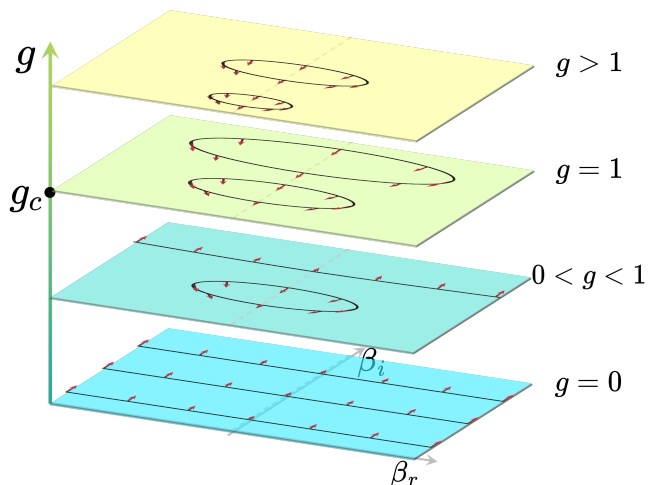


FIG. 1. The continuous lines of Fisher zeros on the complex  $\beta = \beta_r + i\beta_i$  plane for 1DTFIM (schematic). The arrows indicate the velocities of the zeros as the transverse field  $g$  is increased. At  $g = 0$ , the zeros congregate into a set of open lines. As  $g$  increases, closed lines (ovals) of zeros appear, while the open lines shift upwards to larger  $\beta_r$  and eventually vanish at the QCP ( $g = g_c = 1$ ). The closed lines continue to move towards the origin as  $g$  is further increased beyond  $g_c$ .

To establish a correct, complete picture of Fisher zeros across the quantum critical point (QCP), it is desired to have a convenient exact formula of  $Z$  valid for all  $g$  values. Then analytical expressions of  $Z$  in various regions of the complex  $\beta$  plane can be derived to delineate the intricate interplay of quantum and thermal fluctuations.

An even more significant impetus for complex  $Z$  comes from the flurry of experiments on quantum simulators and quantum circuits which prompted the generalization of the notion of phase transitions to time-dependent and

open quantum systems [8]. The complex zeros of the Loschmidt echo amplitude were used to define dynamical phase transition in quench dynamics [9]. Following the discovery of measurement induced phase transitions in nonunitary quantum circuits [10–12], various non-hermitian generalizations of the Ising model have been considered where the coupling constants become complex valued as a result of the non-unitary evolution introduced by measurements. For example, Ref. [13] mapped a non-unitary quantum circuit to a 2D classical Ising model at complex temperature. These developments hint a new era of complex  $Z$  in which the complexification is no longer just a mathematical trick but mandated by experiments to take on physical significance.

This work is inspired by the confluence of these ideas. By exhausting the Fisher zeros for a canonical quantum many-body system, the 1DTFIM, we describe how insights about quantum phase transitions and quantum dynamics can be gleaned from the complex-valued partition functions  $Z(\beta)$ . A few surprising results are obtained. (1) In the thermodynamic limit, the Fisher zeros of 1DTFIM form continuous curves (lines and loops) which move smoothly as the coupling constant  $g$  is tuned. (2) Even though the Fisher zeros never touch the real  $\beta$  axis, the quantum critical point can be unambiguously inferred from either the vanishing of open lines (Fig. 1) or the scaling of low-energy excitations extracted from  $Z$ . (3) We exploit the connection between  $Z$  and the maximally entangled thermofield double (TFD) states [14], which are dual to eternal black holes according to the AdS/CFT correspondence [15], to make analytical predictions about the dynamics of TFD. These include the short-time decay of the survival probability, its periodic oscillation at low temperatures, and the recurrence time at the quantum critical point. (4) We further show that aside from being a useful theoretical device,  $Z$  can be realized and probed in nonunitary quantum circuits where the unitary evolution of the qubits is interspersed with projective measurements and post selection.

Our results are corroborated by exact analytical solution, exact diagonalization, and high order tensor renormalization group (HOTRG) [16]. While these observations are made for 1DTFIM, we conjecture that the regularity of Fisher's zeros and the rich implications of the complex partition function  $Z$  generalize to a host of other many-body systems. Since  $Z$  and its zeros can be reliably computed for relatively small system sizes, the program outlined here can serve as a powerful diagnostic tool for quantum many-body physics.

*Fisher zeros from the exact partition function.* The Hamiltonian of the 1DTFIM can be written as

$$H = - \sum_{i=1}^L (\sigma_i^z \sigma_{i+1}^z + g \sigma_i^x), \quad (1)$$

where  $\sigma_i^x$  and  $\sigma_i^z$  are the Pauli matrix operators on site

$i$ , and the coupling constant  $g$  is the transverse magnetic field measured in units of the nearest neighbor Ising interaction (set to 1). As well known, in the thermodynamic limit ( $L \rightarrow \infty$ ), a quantum phase transition at the critical coupling  $g_c = 1$  separates the ferromagnetic phase ( $g < 1$ ) from the paramagnetic phase ( $g > 1$ ).

While 1DTFIM is exactly solvable, the analytical form of its partition function  $Z$  is subtle to write down. Usually the model is treated in fermionic representation after the Jordan-Wigner transformation, where one has to confront the two sectors (even and odd) of the total fermion number that involve  $L$ -dependence [17]. We find it cleaner to stick to the spin representation and map  $Z = \text{Tr} e^{-\beta H}$  to that of an anisotropic 2D Ising model, and its Onsager-Kaufman solution [18, 19], by Trotter decomposition along the imaginary time axis  $\beta$  which plays the role of another spatial dimension  $y$  [20]. The result is

$$Z = \frac{1}{2} \left[ \prod_{k=1}^L 2 \cosh(\beta \epsilon_{2k}) + \text{sign}(g_c - g) \prod_{k=1}^L 2 \sinh(\beta \epsilon_{2k}) + \prod_{k=1}^L 2 \cosh(\beta \epsilon_{2k-1}) + \prod_{k=1}^L 2 \sinh(\beta \epsilon_{2k-1}) \right], \quad (2)$$

where  $\epsilon_k = [1 + g^2 - 2g \cos(\pi k/L)]^{1/2}$ . We refer to Eq. (2) as the Suzuki solution, even though the all important  $\text{sign}(g_c - g)$  did not appear explicitly in Ref. [20] and perhaps is not widely appreciated. Without the sign factor, one would have expected the KW duality [7], i.e.  $Z$  is invariant under the transformation  $g \rightarrow 1/g$ ,  $\beta \rightarrow g\beta$  so that it is sufficient to analyze the subspace  $g < 1$ . This is only an illusion: the correct formula Eq. (2) shows that  $Z$  itself does not possess KW duality and implies the presence of the recently proposed non-invertible symmetry [21, 22]. The distribution of Fisher zeros on the quantum disordered side  $g > 1$  is qualitatively different from the ordered side  $g < 1$ .

With the form of  $Z$  determined, we now sketch how Fisher zeros are located and visualized. To analytically continue  $Z$ , we simply allow  $\beta$  to be complex,  $\beta = \beta_r + i\beta_i$ , in Eq. (2). On the complex  $\beta$  plane,  $Z(\beta)$  is not a polynomial but an entire function of  $\beta$ . Following Fisher [3], we can factorize  $Z$  into  $Z(\beta) = e^{h(\beta)} \prod_j (\beta - z_j)$  where  $h$  is an entire function, and the multiplicity of  $z_j$ , the  $j$ -th root of  $Z = 0$ , is assumed to be 1. Define the free energy (up to a factor of  $\beta$ ) as  $f = -\ln Z = -h - f_{na}$ , where the non-analytical part  $f_{na} = \sum_j \ln(\beta - z_j)$  develops singularities at  $\beta = z_j$  and is completely determined by the Fisher zeros  $\{z_j\}$ . Let  $f_{na} = \phi + i\psi$ , then real part  $\phi = \sum_i \ln|\beta - z_j|$  can be interpreted as the electric potential due to a set of point charges at  $\{z_j\}$  [4]. The electric field lines stem out of these Fisher charges and correspond to the contour line of the imaginary part  $\psi$  [4]. A branch cut of  $f$  is developed at each Fisher zero. Thus the contour plot of the real and imaginary part of

$f$  can serve as an intuitive way to locate the Fisher zeros, matching the exact solution (Fig. 2). Note that in Fig. 2, due to the mirror symmetry of Fisher zeros with respect to the  $\beta_i$  axis, only the Fisher zeros at the first quadrant is displayed. In the thermodynamic limit, if the Fisher zeros come close to each other, the charge density  $\rho(\beta) = \sum_j \delta(\beta - z_j)$  may become a continuous function.

*Tensor renormalization group with complex  $\beta$ .* We also compute  $Z$  using an independent method which serves two purposes. First, it confirms the analytical solution Eq. (2) is correct. Second, it demonstrates a general and precise technique to compute  $Z(\beta \in \mathbb{C})$  for interacting quantum spin models for which there is no exact solution. Since  $Z$  can be represented as the trace of a product of local tensors, it can be evaluated by tensor network algorithms [23–25] which have proven to be efficient and accurate for spin models [26]. Starting from the 1D system, we first construct a 2D “lattice” of size  $L \times N$  by Trotter decomposition  $\beta = \tau N$ . Then,  $Z$  is obtained from HOTRG. The results are in agreement with both exact diagonalization and the exact solution above.

It is worth to mention that when  $\beta$  is complex, Monte Carlo develops sign problems but HOTRG can yield  $Z$  accurately [26]. Previously renormalization group (RG) transformation has been generalized to the complex  $\beta$  plane to study confinement in lattice gauge theory and classical  $O(N)$  models. It was observed that the Fisher zeros are located at the boundary of the attraction basins of infrared fixed points, and they control the global properties of the complex RG flows [27, 28]. Here we confine our attention to the evaluation of Fisher zeros through HOTRG but for a quantum spin model.

*Motion of Fisher zeros across QCP.* Fig. 1 sketches the evolution of Fisher zeros on the complex  $\beta$  plane as the coupling constant  $g$  is varied. The main observations are summarized into (a) to (d) below. (a) The Fisher zeros of 1DTFIM appear as continuous lines, rather than isolated points or densely packed regions, in the thermodynamic limit  $L \rightarrow \infty$ . (b) For  $g < 1$ , there exist *open lines* of zeros that are approximately parallel to the  $\beta_r$  axis. (c) As  $g$  increases from 0 to 1, these open lines shift upwards toward large  $\beta_i$ , and vanish completely at the QCP  $g = 1$ . (d) Away from  $g = 0$ , *closed loops* of Fisher zeros also appear and persist for all  $g$ . These loops are centered around the  $\beta_i$  axis and move towards  $\beta_i = 0$  as  $g$  is increased. We stress that properties (a) to (d) came as surprises, in the sense that they are not obvious from staring at the model or the exact solution of  $Z$ .

Some of these features can be appreciated by considering a few limit cases. At  $g = 0$ ,  $Z = \text{Tr}V^L$  where the transfer matrix  $V = e^\beta + \sigma_x e^{-\beta}$ . The Fisher zeros are determined by the condition  $\tanh \beta = e^{in\pi/L}$  with  $n$  an integer, i.e. they are uniformly distributed on the unit circle on the plane of  $\tanh \beta$  [13]. On the complex  $\beta$  plane, the zeros form a set of straight lines at  $\beta_i = \pi/4 + m\pi$ , with  $m$  an integer, as  $L \rightarrow \infty$ . Another simple case is

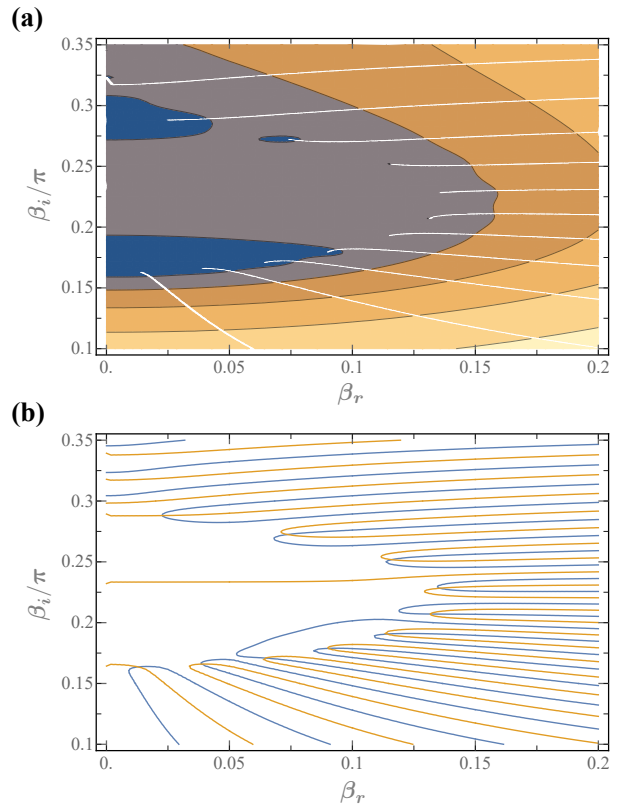


FIG. 2. Locating Fisher zeros. (a) The contour lines of Ref. The white lines indicate the branch cuts, which terminate the Fisher zeros at the starting points ( $L = 32, g = 1.8$ ). (b) Zeros of the same system determined by the intersections of  $\text{Re}(Z) = 0$  and  $\text{Im}(Z) = 0$ .

the small size system with  $L = 2$ . After some algebra, one finds the zeros are located on the  $\beta_i$  axis at

$$\beta_i = (m + \frac{1}{2})\pi / (\sqrt{1 + g^2} \pm 1)$$

where  $m$  again is an integer. While the size  $L = 2$  is too small to feature Fisher zeros away from the  $\beta_i$  axis or the closed loops, it does correctly capture the trend that the zeros move toward  $\beta_i = 0$  as  $g$  is increased.

It is clear from (d) that the QCP is marked by a qualitative change in the Fisher zeros. To describe the lowest open Fisher line, one can take its imaginary part  $\beta_i$  at some fixed large value of  $\beta_r$  and plot  $1/\beta_i$  against  $g$ . In Ref. [5], it was shown that the resulting curve is linear near QCP. Similarly, for the closed Fisher lines, we can select a characteristic point on each curve, e.g. recording the  $\beta_i$  value of the rightmost point. Then a linear relationship between  $1/\beta_i$  and  $g$  is observed on the quantum disordered side  $g > 1$ , which is consistent with the spin flip excitations. A more refined description is to define the velocities of the zeros on the complex  $\beta$  plane with increasing  $g$ . Interestingly, the speed of the zeros exhibits properties similar to the Grüneisen parameter [29, 30].

In the next section, we will describe another way to determine the QCP from the asymptotic oscillations of  $Z$  at low temperatures, which gives consistent results. We conjecture that in general the distribution of Fisher zeros must undergo a qualitative change at QCP. Otherwise, the two quantum phases separated by the QCP would share the same global patterns of RG flows on the complex  $\beta$  plane, which would contradict to the fact that the two phases correspond to different RG fixed points.

*What can  $Z$  tell us about quantum dynamics?* We now switch perspective to view  $Z$  as the survival amplitude of certain quantum state. Let  $\beta = \beta_r + it$ , and interpret the imaginary (real) part of  $\beta$  as time  $t$  (the inverse temperature  $\beta_r = 1/k_B T$ ). Let  $E_n$  be the eigen energies, and  $|n\rangle$  the corresponding eigen states, of Hamiltonian  $H$ . Then

$$Z(\beta_r, t) = \sum_n e^{-\beta_r E_n} e^{-i E_n t}$$

describes the unitary dynamics of a mixed ensemble. The modulus square of  $Z$  defines the spectral form factor

$$S(\beta_r, t) = \left| \frac{Z(\beta_r, t)}{Z(\beta_r, 0)} \right|^2$$

which is normalized to 1 as  $t = 0$ . The disorder average of  $S$  has been used to diagnose chaos and information scrambling in Hamiltonians containing random couplings, e.g. the SYK model [31]. Following Ref. [32], we purify the mixed state above by introducing the thermofield double state in an enlarged Hilbert space

$$|\psi(\beta_r, 0)\rangle = \frac{1}{\sqrt{Z(\beta_r, 0)}} \sum_n e^{-\beta_r E_n/2} |n\rangle_L \otimes |n\rangle_R$$

where for clarity the subscripts  $L, R$  are used to denote the left and right copy respectively [14]. Under the single Hamiltonian  $H_L \otimes 1_R$ , the TFD state evolves with time as  $\psi(\beta_r, t) = e^{-it(H_L \otimes 1_R)} |\psi(\beta_r, 0)\rangle$ . One finds that  $S$  is nothing but the survival probability [32]

$$S(\beta_r, t) = |\langle \psi(\beta_r, t) | \psi(\beta_r, 0) \rangle|^2$$

In contrast to the Loschmidt echo in quench dynamics [9], here the connection between  $Z$  and quantum dynamics is established by the TFD states, which are dual to the eternal black hole in the context of AdS/CFT correspondence [15]. Via this bridge, the detailed knowledge about the analytical structure of  $Z$ , including the Fisher zeros, can now be translated into new insights about quantum dynamics. Three examples are given below.

The short time dynamics of  $S$  is characterized by exponential decay  $S(t) \simeq e^{-(t/\tau)^2}$  with  $\tau^2 = k_B \beta_r / C_V$ . Fig. 3(a) shows the specific heat capacity  $C_V/L$  obtained by fitting  $S(t)$  at some typical values of  $g$ . The decay rate  $1/\tau \propto \sqrt{C_V}$  correlates with the locations of Fisher zeros at which  $S$  is forced to vanish. This can be seen on the low  $\beta_r$  portion of Fig. 3(a): as  $g$  is increased from  $g = 1$ ,

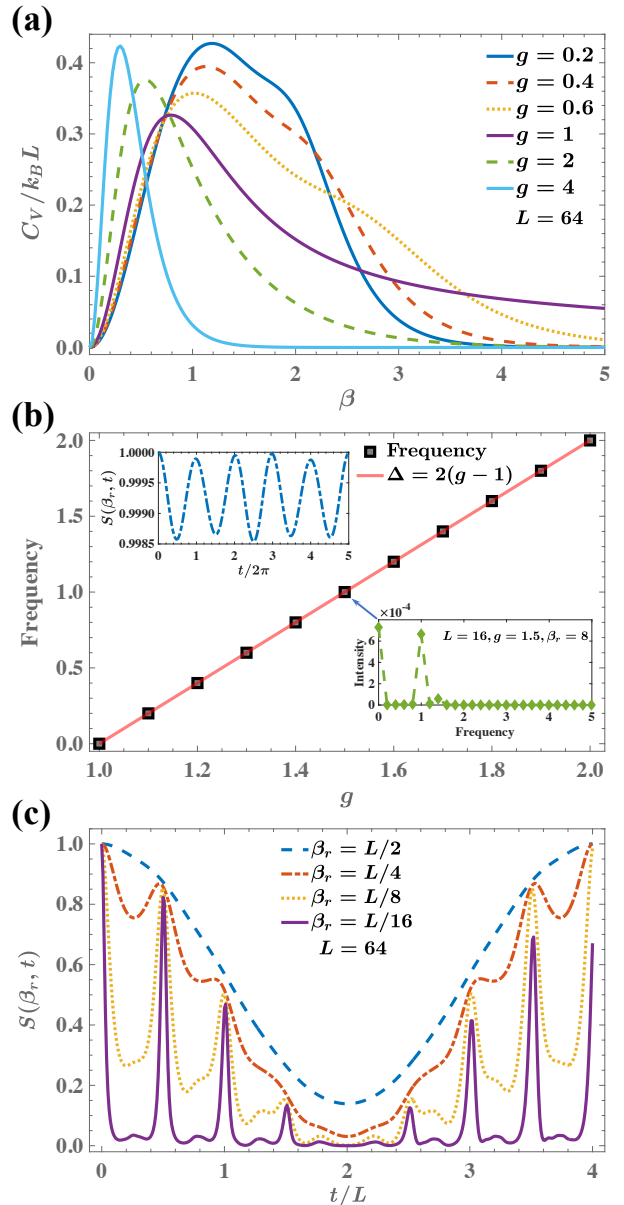


FIG. 3. The rich behaviors of the spectral form factor (survival probability)  $S(\beta_r, t)$ . (a) The short-time decay of  $S$  is dictated by the specific heat capacity  $C_V/L$ . (b) The low temperature oscillations (inset,  $g = 1.5$ ) of  $S$ . The oscillation frequency obtained from Fourier transform can be fit by  $\Delta = 2(g - 1)$  and vanishes at QCP. (c) Fine structures of  $S$  over long time scales for different  $\beta_r$ . At the QCP, all exhibit the same periodicity  $t^* = 4L$ , the quantum recurrence time.

the Fisher zeros move closer to the  $\beta_r$  axis, and accordingly  $S$  is suppressed from 1 to zero at an increasing rate. At high  $\beta_r$  (low temperatures), however, the decay is most rapid at the QCP, where quantum fluctuation is strong and  $C_V$  reaches maximum.

The long time behavior of  $S(t)$  is complicated but simplicity emerges at low temperatures. To understand

this, we can convert the products of hyperbolic sines and cosines in the exact solution of  $Z$  into sums and expand them for large  $\beta_r$ . The leading contributions to  $S(t)$  are

$$S(t) \simeq 1 + 2e^{-\beta_r \Delta} \cos(\Delta t) + \dots$$

where the oscillation frequency  $\Delta = \sum_k (\epsilon_{2k-1} - \epsilon_{2k})$  has the meaning of the excitation gap. Previously in Ref. [5], it was noted from numerics that for  $g \leq 1$  the oscillation frequency vanishes at the QCP while the oscillation amplitude reaches maximum. The analytic asymptote derived here not only explains this observation but also expands its validity to the disordered side  $g \geq 1$  [Fig. 3(b)]. It seems quite general that the low temperature oscillations of  $Z(\beta_r, t)$  can be used to identify QCP.

The dynamics at the QCP exhibits an interesting scaling behavior and a rather rich fine structure. For a system of finite size  $L$ , the energy spectrum is discrete and the initial TFD state will come back to itself after the quantum recurrence time  $t^*$ . Previously, it was claimed that  $t^* = 8L$  [17]. Here our numerical and analytical calculations consistently predict  $t^* = 4L$ . For example, take the limit of large  $\beta_r$ , expand the exact Suzuki solution and carry out the  $k$ -sum, we find at  $g = 1$  the oscillation frequency is  $\Delta = 2 \tan(\pi/4L)$  which becomes  $\pi/2L$  in the limit of large  $L$  to yield  $t^* = 4L$ . As shown in Fig. 3(c), for smaller  $\beta_r$ ,  $S(t)$  deviates significantly from the sinusoidal form to acquire fine structures, but  $t^*$  stays approximately the same. We also observe that at the QCP and for intermediate or large  $(\beta_r, t)$ ,  $S$  exhibits self-similarity, i.e.  $S(\beta_r, t)_L \approx S(n\beta_r, nt)_{nL}$  with  $n$  an integer. This is consistent with the notion of criticality and provides a nice way to define RG flow in the complex plane (see Supplementary Materials).

*Probing  $Z$  from monitored quantum circuits.* Lastly we show that  $Z$  is not just a formal theoretical construct, it can be realized and probed in quantum circuits. Consider an array of qubits,  $j = 1, 2, \dots, L$ . The standard single- and two-qubit Pauli gates implement unitary evolution such as  $U_{zz}(t) = \exp(it \sum_j \sigma_j^z \sigma_{j+1}^z)$  and  $U_x(t) = \exp(itg \sum_j \sigma_j^x)$ . Let us define the cycle operator  $U_F(t) = U_{zz}(t)U_x(t)$ , then repeated application of  $U_F$  produces the time evolution corresponding to the 1DTFIM Hamiltonian, albeit in discretized form  $U(t) = [U_F(t/N)]^N$ . Now let us introduce nonunitary gates in the form of  $U_x(i\beta_r)$  and  $U_{zz}(i\beta_r)$ , i.e. by replacing  $t$  with the imaginary time  $i\beta_r$ . These gates can be realized by including ancilla qubits and performing projective measurements and post-selection on the ancilla [33–35], where the value of  $\beta_r$  characterizes the strength of the measurement. If we intersperse these unitary and nonunitary gates [8], e.g. by forming a cycle

$$U_F(\beta_r, t) = U_x(i\beta_r)U_x(t)U_{zz}(i\beta_r)U_{zz}(t),$$

the resulting evolution operator yields exactly  $Z(\beta_r, t) = [U_F(\beta_r/N, t/N)]^N$  in the limit of large  $N$ . From this

perspective,  $Z(\beta_r, t)$  describes the competition between unitary time evolution and quantum measurement in an open quantum many-body system.

The circuit construction here differs from the approach in Ref. [13] based on the transfer matrix. From an alternative perspective, the nonunitary gates introduce imaginary parts to the coupling constants in the Hamiltonian and render it non-hermitian [36]. Previous studies on non-hermitian Ising-type models mostly focused on their entanglement or spectral properties [33–35]. Given the recent success in observing Lee-Yang zeros [37] and Loschmidt ratios [38], it seems promising that the circuit connection to  $Z$  and TFD states [39] can lead to future experimental studies of Fisher zeros [40].

In summary, this work presents a comprehensive analysis of the Fisher zeros in the 1DTFIM. We have demonstrated that Fisher zeros form continuous, smoothly shifting curves in the complex  $\beta$  plane, and they offer insights into quantum criticality despite never touching the real  $\beta$  axis. The complex partition function  $Z$  provides valuable analytical predictions about the quantum dynamics which is beyond the reach of the traditional thermodynamics, and can be realized and probed in nonunitary quantum circuits. Our improvement/clarification over the original Suzuki solution correctly captures the different excitations on the two sides of the QPT and the breakdown of the Kramers-Wannier duality. These findings demonstrate the power of this approach, and open up a new avenue to study quantum critical systems in 1D [41–43] and higher dimensions [44–46].

We thank Youjin Deng, Shijie Hu, Ian McCulloch, Yannick Meurice, Tao Xiang, and Jiahao Yang for helpful discussions. This work is supported by National Natural Science Foundation of China (Grant No. 12274126). EZ acknowledges the support from NSF grant PHY-206419 and AFOSR grant FA9550-23-1-0598.

---

\* ezhao2@gmu.edu

† hyzou@phy.ecnu.edu.cn

- [1] C. N. Yang and T. D. Lee, Statistical theory of equations of state and phase transitions. i. theory of condensation, *Phys. Rev.* **87**, 404 (1952).
- [2] T. D. Lee and C. N. Yang, Statistical theory of equations of state and phase transitions. ii. lattice gas and ising model, *Phys. Rev.* **87**, 410 (1952).
- [3] M. Fisher and W. Brittin, Statistical physics, weak interactions, field theory, Lectures in Theoretical Physics (Boulder: University of Colorado Press) vol VIIC (1965).
- [4] I. Bena, M. Droz, and A. Lipowski, Statistical mechanics of equilibrium and nonequilibrium phase transitions: the yang-lee formalism, *International Journal of Modern Physics B* **19**, 4269 (2005).
- [5] Y. Liu, S. Lv, Y. Yang, and H. Zou, Signatures of quantum criticality in the complex inverse temperature plane, *Chinese Physics Letters* **40**, 050502 (2023).

- [6] S. Sachdev, *Quantum Phase Transitions* (Cambridge University Press, Cambridge, 2011).
- [7] H. A. Kramers and G. H. Wannier, Statistics of the two-dimensional ferromagnet. part i, *Phys. Rev.* **60**, 252 (1941).
- [8] M. P. Fisher, V. Khemani, A. Nahum, and S. Vijay, Random quantum circuits, *Annual Review of Condensed Matter Physics* **14**, 335 (2023).
- [9] M. Heyl, A. Polkovnikov, and S. Kehrein, Dynamical quantum phase transitions in the transverse-field ising model, *Phys. Rev. Lett.* **110**, 135704 (2013).
- [10] Y. Li, X. Chen, and M. P. A. Fisher, Quantum zeno effect and the many-body entanglement transition, *Phys. Rev. B* **98**, 205136 (2018).
- [11] B. Skinner, J. Ruhman, and A. Nahum, Measurement-induced phase transitions in the dynamics of entanglement, *Phys. Rev. X* **9**, 031009 (2019).
- [12] A. Chan, R. M. Nandkishore, M. Pretko, and G. Smith, Unitary-projective entanglement dynamics, *Phys. Rev. B* **99**, 224307 (2019).
- [13] S. Basu, D. P. Arovas, S. Gopalakrishnan, C. A. Hooley, and V. Oganesyan, Fisher zeros and persistent temporal oscillations in nonunitary quantum circuits, *Phys. Rev. Res.* **4**, 013018 (2022).
- [14] Y. Takahashi and H. Umezawa, Thermo field dynamics, *International journal of modern Physics B* **10**, 1755 (1996).
- [15] J. Maldacena, Eternal black holes in anti-de sitter, *Journal of High Energy Physics* **2003**, 021 (2003).
- [16] Z. Y. Xie, J. Chen, M. P. Qin, J. W. Zhu, L. P. Yang, and T. Xiang, Coarse-graining renormalization by higher-order singular value decomposition, *Phys. Rev. B* **86**, 045139 (2012).
- [17] Nivedita, H. Shackleton, and S. Sachdev, Spectral form factors of clean and random quantum ising chains, *Phys. Rev. E* **101**, 042136 (2020).
- [18] L. Onsager, Crystal statistics. i. a two-dimensional model with an order-disorder transition, *Phys. Rev.* **65**, 117 (1944).
- [19] B. Kaufman, Crystal statistics. ii. partition function evaluated by spinor analysis, *Phys. Rev.* **76**, 1232 (1949).
- [20] M. Suzuki, Relationship between d-dimensional quantum spin systems and (d+1)-dimensional ising systems: Equivalence, critical exponents and systematic approximants of the partition function and spin correlations, *Progress of Theoretical Physics* **56**, 1454 (1976).
- [21] N. Seiberg and S.-H. Shao, Majorana chain and Ising model - (non-invertible) translations, anomalies, and emanant symmetries, *SciPost Phys.* **16**, 064 (2024).
- [22] T. Senthil, Symmetries without an inverse: An illustration through the 1+1-d ising model (2024), *Journal Club for Condensed Matter Physics: 10.36471/JCCM-February-2024-03*.
- [23] R. Orús, A practical introduction to tensor networks: Matrix product states and projected entangled pair states, *Annals of Physics* **349**, 117 (2014).
- [24] J. I. Cirac, D. Pérez-García, N. Schuch, and F. Verstraete, Matrix product states and projected entangled pair states: Concepts, symmetries, theorems, *Rev. Mod. Phys.* **93**, 045003 (2021).
- [25] Y. Meurice, R. Sakai, and J. Unmuth-Yockey, Tensor lattice field theory for renormalization and quantum computing, *Rev. Mod. Phys.* **94**, 025005 (2022).
- [26] A. Denblyker, Y. Liu, Y. Meurice, M. P. Qin, T. Xiang, Z. Y. Xie, J. F. Yu, and H. Zou, Controlling sign problems in spin models using tensor renormalization, *Phys. Rev. D* **89**, 016008 (2014).
- [27] A. Denblyker, D. Du, Y. Liu, Y. Meurice, and H. Zou, Fisher's zeros as the boundary of renormalization group flows in complex coupling spaces, *Phys. Rev. Lett.* **104**, 251601 (2010).
- [28] Y. Meurice and H. Zou, Complex renormalization group flows for 2d nonlinear  $o(n)$  sigma models, *Phys. Rev. D* **83**, 056009 (2011).
- [29] L. Zhang, Universal thermodynamic signature of self-dual quantum critical points, *Phys. Rev. Lett.* **123**, 230601 (2019).
- [30] L. Zhang and C. Ding, Finite-size scaling theory at a self-dual quantum critical point, *Chinese Physics Letters* **40**, 010501 (2023).
- [31] J. S. Cotler, G. Gur-Ari, M. Hanada, J. Polchinski, P. Saad, S. H. Shenker, D. Stanford, A. Streicher, and M. Tezuka, Black holes and random matrices, *Journal of High Energy Physics* **2017**, 1 (2017).
- [32] A. del Campo, J. Molina-Vilaplana, and J. Sonner, Scrambling the spectral form factor: Unitarity constraints and exact results, *Phys. Rev. D* **95**, 126008 (2017).
- [33] E. Granet, C. Zhang, and H. Dreyer, Volume-law to area-law entanglement transition in a nonunitary periodic gaussian circuit, *Phys. Rev. Lett.* **130**, 230401 (2023).
- [34] V. Ravindranath and X. Chen, Robust oscillations and edge modes in nonunitary floquet systems, *Phys. Rev. Lett.* **130**, 230402 (2023).
- [35] L. Su, A. Clerk, and I. Martin, Dynamics and phases of nonunitary floquet transverse-field ising model, *Phys. Rev. Res.* **6**, 013131 (2024).
- [36] C. M. Bender and S. Boettcher, Real spectra in non-hermitian hamiltonians having pt symmetry, *Phys. Rev. Lett.* **80**, 5243 (1998).
- [37] X. Peng, H. Zhou, B.-B. Wei, J. Cui, J. Du, and R.-B. Liu, Experimental observation of lee-yang zeros, *Phys. Rev. Lett.* **114**, 010601 (2015).
- [38] P. Jurcevic, H. Shen, P. Hauke, C. Maier, T. Brydges, C. Hempel, B. P. Lanyon, M. Heyl, R. Blatt, and C. F. Roos, Direct observation of dynamical quantum phase transitions in an interacting many-body system, *Phys. Rev. Lett.* **119**, 080501 (2017).
- [39] D. Zhu, S. Johri, N. M. Linke, K. Landsman, C. Huerta Alderete, N. H. Nguyen, A. Matsuura, T. Hsieh, and C. Monroe, Generation of thermofield double states and critical ground states with a quantum computer, *Proceedings of the National Academy of Sciences* **117**, 25402 (2020).
- [40] B.-B. Wei, S.-W. Chen, H.-C. Po, and R.-B. Liu, Phase transitions in the complex plane of physical parameters, *Scientific Reports* **4**, 10.1038/srep05202 (2014).
- [41] X. Chen, Z.-C. Gu, Z.-X. Liu, and X.-G. Wen, Symmetry protected topological orders and the group cohomology of their symmetry group, *Phys. Rev. B* **87**, 155114 (2013).
- [42] H. Zou, E. Zhao, X.-W. Guan, and W. V. Liu, Exactly solvable points and symmetry protected topological phases of quantum spins on a zig-zag lattice, *Phys. Rev. Lett.* **122**, 180401 (2019).
- [43] Q. Zheng, X. Li, and H. Zou, Symmetry-protected topological phase transitions and robust chiral order on a tunable zigzag lattice, *Phys. Rev. B* **101**, 165131 (2020).
- [44] Z. Zhu, D. A. Huse, and S. R. White, Unexpected z-direction ising antiferromagnetic order in a frustrated spin-1/2  $J_1 - J_2$   $xy$  model on the honeycomb lattice, *Phys.*



Rev. Lett. **111**, 257201 (2013).

[45] W.-Y. Liu, S.-S. Gong, Y.-B. Li, D. Poilblanc, W.-Q. Chen, and Z.-C. Gu, Gapless quantum spin liquid and global phase diagram of the spin-1/2 j1-j2 square antiferromagnetic heisenberg model, Science Bulletin **67**, 1034 (2022).

[46] H. Zou, F. Yang, and W. Ku, Nearly degenerate ground states of a checkerboard antiferromagnet and their bosonic interpretation, Sci. China Phys. Mech. Astron. **67**, 217211 (2024).

---

## Supplemental Materials for “Exact Fisher zeros and thermofield dynamics across a quantum critical point”

### DISCUSSION ON THE SUZUKI SOLUTION

#### Numerical check of original Suzuki solution

The original Suzuki solution [S1] of the partition function is

$$Z_{\text{su}} = \frac{1}{2} \left[ \prod_{k=1}^L 2 \cosh(\beta \epsilon_{2k}) + \prod_{k=1}^L 2 \sinh(\beta \epsilon_{2k}) + \prod_{k=1}^L 2 \cosh(\beta \epsilon_{2k-1}) + \prod_{k=1}^L 2 \sinh(\beta \epsilon_{2k-1}) \right]. \quad (\text{S1})$$

where the Kramers-Wannier (KW) [S2] is fully manifested; specifically, Eq. S1 remains invariant under the transformation  $g \rightarrow 1/g$ ,  $\beta \rightarrow \beta g$ . Consequently, the Fisher zero results for  $g > 1$  can be easily derived by mapping to the dual space ( $g < 1$ ). Therefore, zero lines will reappear for  $g > 1$  to characterize the dual spin flip excitations, similar to those for domain walls. Figure S1(a) shows the results of Fisher zeros at  $g = 1.5$  for  $L = 16$  and in the thermodynamic limit, according to the Suzuki solution and the exact formula given in Ref. [S3], thereby illustrating the KW duality behavior between spin flips and domain walls on the two sides of the QCP in the complex  $\beta$  plane.

To verify whether the physical picture at  $g > 1$  obtained from the Suzuki solution is correct, we employ two precise numerical methods, ED and tensor network calculations, to obtain Fisher zeros solutions for the same small system with  $L = 16$ . In the tensor network calculations, we first construct a 2D lattice of size  $L \times n$  from the 1D system by using Trotter decomposition with  $\beta = \tau n$ , then solve the partition function using the higher-order tensor renormalization group (HOTRG) method [S4], an efficient tensor network algorithm capable of handling sign problems in the complex  $\beta$  plane [S5]. In our HOTRG calculations,  $n = 1000$ , and the bond dimension  $D_b$  describing the entanglement properties is set to 32. We find that the ED and the HOTRG calculations provide consistent results [Fig. S1(b)], but they are entirely inconsistent with the picture from the Suzuki solution with the same system size  $L = 16$ . In the latter two numerical results, there is no reappearance of Fisher zero lines in the complex  $\beta$  plane; instead, only localized Fisher zero structures are found [Fig. S1(b)], indicating the presence of closed zero curves in the thermodynamic limit. This implies that a new description is needed for spin flip excitations in the quantum disordered phase on the complex  $\beta$  plane, as the Fisher zero lines strictly adhering to KW duality according to the Suzuki solution will no longer apply.

#### Modified Suzuki solution at quantum disordered side

In this section, we discuss the reasons for the discrepancy between results from the Suzuki solution and those from the unbiased numerical calculations. Prior to deriving Eq. S1, anisotropic Onsager/Kaufman results are used, with the Trotter step  $n$  tends to infinity:

$$Z = \lim_{n \rightarrow \infty} \frac{1}{2} \left[ \prod_{k=1}^L 2 \cosh\left(\frac{n}{2} \gamma_{2k}\right) + \prod_{k=1}^L 2 \sinh\left(\frac{n}{2} \gamma_{2k}\right) + \prod_{k=1}^L 2 \cosh\left(\frac{n}{2} \gamma_{2k-1}\right) + \prod_{k=1}^L 2 \sinh\left(\frac{n}{2} \gamma_{2k-1}\right) \right], \quad (\text{S2})$$

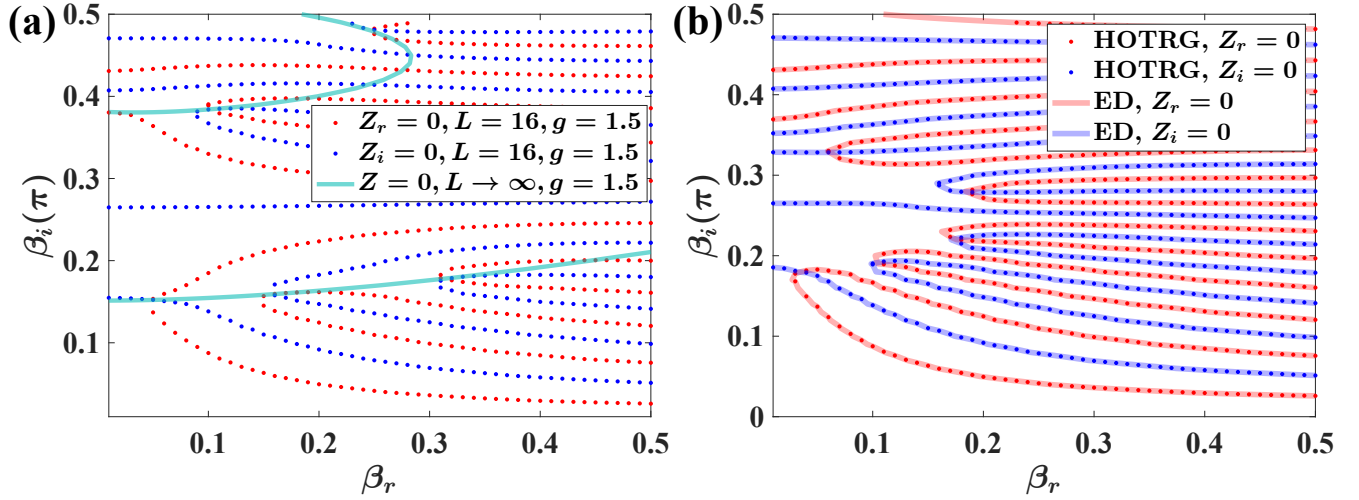


FIG. S1. Fisher zero results obtained from three methods at  $g = 1.5$ . (a) Fisher zeros for the system with  $L = 16$  and in the thermodynamic limit obtained using the Suzuki solution. The red and blue dots represent the values where the real ( $Z_r$ ) and imaginary ( $Z_i$ ) parts of the partition function become zero for  $L = 16$ , respectively. Their intersections yield the Fisher zeros. The green line represents the Fisher zeros in the thermodynamic limit. The discrete Fisher zeros for  $L = 16$  roughly lie on the continuous curve in the thermodynamic limit. (b) The red (blue) dots represent the results of the real (imaginary) parts of the partition function obtained using HOTRG for  $L = 16$ , while the red (blue) lines represent the results obtained using ED. The Fisher zeros obtained by the two methods are in complete agreement.

where  $\gamma_k$  is given by

$$\begin{aligned} \cosh \gamma_k &= \cosh\left(\frac{2}{n}\beta g\right) \cosh\left(\frac{2}{n}\beta\right) \\ &\quad - \sinh\left(\frac{2}{n}\beta g\right) \sinh\left(\frac{2}{n}\beta\right) \cos\left(\frac{\pi k}{L}\right). \end{aligned} \quad (\text{S3})$$

The two largest eigenvalues  $\lambda_{\pm}$  provide the majority contribution to the partition function, with  $Z \sim \lambda_+^n + \lambda_-^n$  and

$$\begin{aligned} \lambda_+ &= \exp\left[\frac{1}{2}(\gamma_1 + \gamma_3 + \cdots + \gamma_{2L-1})\right], \\ \lambda_- &= \exp\left[\frac{1}{2}(\gamma_2 + \gamma_4 + \cdots + \gamma_{2L})\right]. \end{aligned} \quad (\text{S4})$$

Differing from the ordered side, where the system has a degeneracy of two, on the quantum disordered side, the system has a degeneracy of only one. This can be addressed by selecting opposite signs for  $\gamma_{2L}$  on different sides, thereby ensuring that  $\lambda_-/\lambda_+ = 1$  for  $g < g_c$  and  $\lambda_-/\lambda_+ < 1$  for  $g > g_c$ . Therefore, at  $n \rightarrow \infty$ ,  $\gamma_k = 2\beta\epsilon_k/n$ , except for  $\gamma_{2L} = 2\beta\epsilon_0/n$  at  $g < g_c$  and  $\gamma_{2L} = -2\beta\epsilon_0/n$  at  $g > g_c$ , respectively. Actually, substituting the specific form of  $\epsilon_0$  into  $\gamma_{2L}$  makes it easier to understand. In this case,  $\gamma_{2L} = 2\beta(g_c - g)/n$ . From an algebraic perspective, the old form  $\gamma_{2L} = 2\beta|g_c - g|/n$  is symmetric at the QCP but not differentiable, leading to the reappearance of zero lines at  $g > g_c$  and creating a fake illusion of KW duality on the complex  $\beta$  plane. Then the exact Suzuki solution at  $g > g_c$  need to modify as

$$\begin{aligned} Z'_{\text{su}} &= \frac{1}{2} \left[ \prod_{k=1}^L 2 \cosh(\beta\epsilon_{2k}) - \prod_{k=1}^L 2 \sinh(\beta\epsilon_{2k}) \right. \\ &\quad \left. + \prod_{k=1}^L 2 \cosh(\beta\epsilon_{2k-1}) + \prod_{k=1}^L 2 \sinh(\beta\epsilon_{2k-1}) \right]. \end{aligned} \quad (\text{S5})$$

In Fig. S2, the modified Suzuki solution Eq. S5 yields the correct picture of Fisher zeros, consistent with those from other two numerical results.



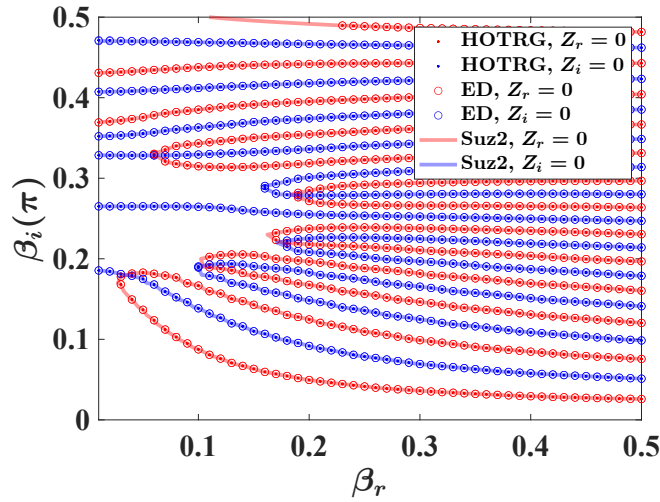


FIG. S2. Fisher zeros obtained from three different methods for  $L = 16$  and  $g = 1.5$ . The results obtained using the modified Suzuki solution (lines) perfectly match those from HOTOGR (dots) and ED (circles).

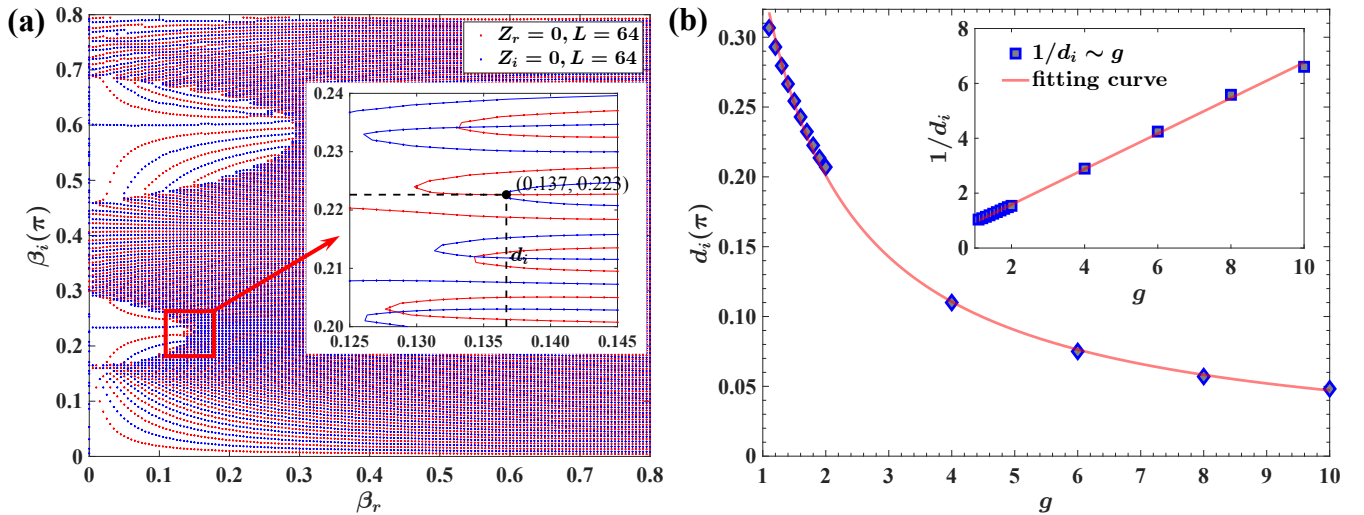


FIG. S3. The Fisher zeros obtained from HOTOGR at  $L = 64$ . (a) An example of the Results at  $g = 1.8$ . The intersections of red (blue) points determine the location of the Fisher zeros. The zeros are densely distributed and approximate form closed curve structures. The inset illustrates the distance  $d_i$  from the rightmost point of the first approximate curve to the real  $\beta$  axis. (b) The distance  $d_i$  obtained at different  $g$  values exhibits an inverse proportionality with  $g$ . The inset depicts the fit with  $0.65(g + 0.45)$ .

### FISHER ZEROS SOLUTION AND VELOCITY OF ZEROS IN THE THERMODYNAMIC LIMIT

In the thermodynamic limit, the solution of  $Z_{\text{su}} = 0$  at  $g < 1$  can be written as [S3]

$$\tilde{S} = \int_0^\pi \log |\tanh(\beta \epsilon_q)|^2 dq = 0 \quad (\text{S6})$$

where  $\epsilon_q = (1 + g^2 - 2g \cos q)^{1/2}$ . Due to the different signs of the sinh terms containing  $\epsilon_{2k}$  and  $\epsilon_{2k-1}$ ,  $\tilde{S}$  at  $g > 1$  in the thermodynamic limit is difficult to express in a simple form. However, we can still obtain an asymptotic solution in the thermodynamic limit using the solution for large  $L$ . Therefore, we formally represent the solution for the zeros as  $\tilde{S}(\beta, g) = 0$ . When  $g$  undergoes a slight change to  $g'$ , the zero moves to  $\beta'$  in the complex plane, resulting in  $\tilde{S}(\beta', g') = 0$ . By performing a Taylor expansion of  $\tilde{S}$  at  $(\beta, g)$  up to the first order, we obtain the velocity of the

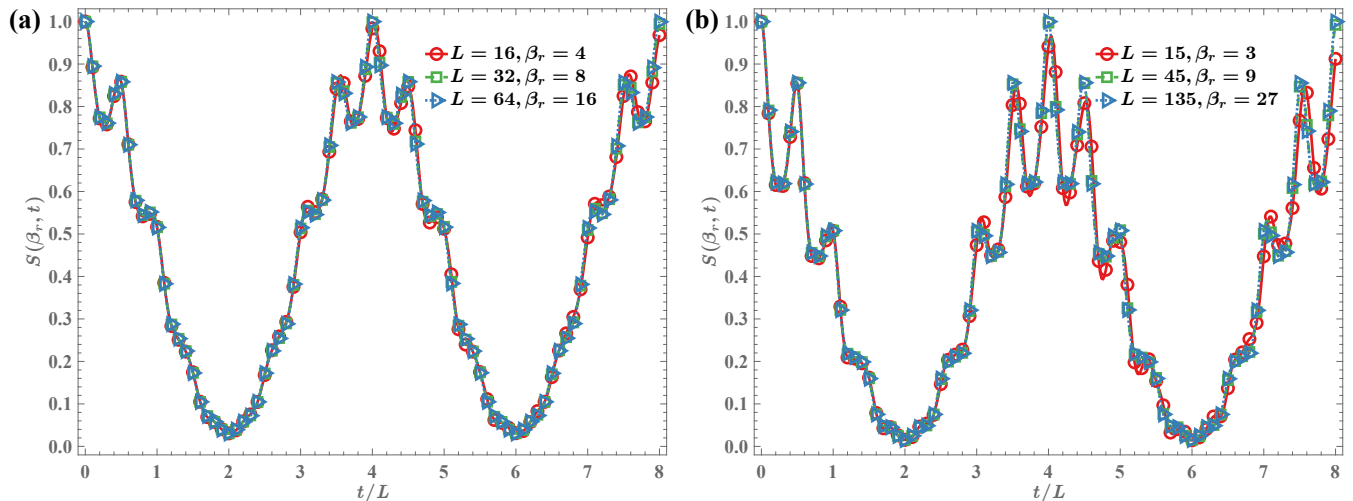


FIG. S4. The oscillatory behavior of  $S$  at different  $L$  values not only exhibits the same periodicity but also shows nearly perfect overlap, demonstrating self-similar behavior. Examples with (a)  $n = 2$  and (b)  $n = 3$ .

zeros' movement in the complex  $\beta$  plane with respect to changes in  $g$ :

$$v_g = \frac{\partial \beta}{\partial g} = - \left( \frac{\partial \tilde{S}}{\partial g} \right)_{\beta} / \left( \frac{\partial \tilde{S}}{\partial \beta} \right)_g \quad (\text{S7})$$

which is similar to the Grüneisen parameter. At the critical point, the zeros on the closed Fisher curve have a finite speed, while on the open Fisher curve, the speed of the zeros diverges at large  $\beta$  and in the thermodynamic limit. These conclusions are consistent with the behavior of the Grüneisen parameter at the critical point [S6, S7].

### SCALING OF THE ZEROS

As mentioned in the text, the zeros of the partition function can be located numerically by tensor network calculation. We can determine the positions of these zeros under fixed  $\beta_r$  by scanning  $Z$  with respect to  $\beta_i$ . Figure S3(a) illustrates several examples at  $L = 64$  and  $g = 1.8$ . Our numerical results from HOTRG are consistent with the exact solutions. As  $L$  increases, the zeros indeed become denser and tend toward some closed curves. By comparing the approximate zero curves for different  $g$  values, we find that as  $g$  increases, the size of the closed curve gradually decreases and approaches the real axis. Since the inverse of imaginary part of  $\beta$  ( $1/\beta_i$ ) provides the energy scale of quantum fluctuations [S3], we choose the distance  $d_i$  from the rightmost point of the zero curve closest to the real axis to the real axis for scaling. We find that as  $g$  increases, this distance  $d_i$  decreases inversely with  $g$  [Fig. S3(b)]. This scaling relationship is consistent with the linear relation between the spin flip excitation gap  $\Delta$  and  $g$ . Therefore, on the quantum disordered side, the size of closed Fisher zero curves can be used to characterize spin flip excitations, while Fisher zero lines used to characterize domain walls on the ordered side. The different manifestations of excitations on Fisher zeros on the two sides of the QCP indicate that the KW duality does not necessarily enforce similarities in the behaviors of the renormalized classical side and the quantum disorder side in the complex  $\beta$  plane.

### SELF SIMILARITY OF $S$

Self-similarity is a fundamental characteristic of quantum critical points, reflecting the scale-invariant nature of quantum fluctuations at these points. The relationship  $S(\beta_r, t)_L \approx S(n\beta_r, nt)_{nL}$  at  $g_c = 1$  provides a classic example of how systems at different scales can exhibit similar behavior. This property can be used for RG analysis, a powerful tool in studying critical phenomena. Figure S4 illustrates the self-similar behavior of  $S$  using  $n = 2$  and  $n = 3$  as examples. The oscillatory behavior of  $S$  at different  $L$  values not only exhibits the same periodicity but also shows nearly perfect overlap, demonstrating the self-similar nature. The self-similarity implies that the critical exponents, which characterize the behavior of physical quantities near the QCP, are scale-invariant.

Similar to correlation functions,  $S$  can be used for two-lattice matching RG analysis. In-depth analysis of the RG flow derived from this self-similarity relationship sheds light on the underlying mechanisms governing quantum phase transitions. By matching  $S(\beta)_L=S(\beta')_{L'}$  from the system with size  $L$  to  $L'$ , we can define an RG flow  $\beta \rightarrow \beta'$  in the complex plane. This flow starts from large  $\beta$  region and can reach small  $\beta$ , until the singularity near the Fisher zeros disrupt the self-similar behavior. By observing the trajectory of  $\beta$  in the complex plane as it transforms into  $\beta'$ , one can map the evolution of the system across different scales. This mapping not only validates the theoretical predictions of critical phenomena but also provides a quantitative tool to explore the dynamics of quantum critical systems.

---

\* ezhao2@gmu.edu

† hyzou@phy.ecnu.edu.cn

- [S1] M. Suzuki, Relationship between d-dimensional quantal spin systems and (d+1)-dimensional ising systems: Equivalence, critical exponents and systematic approximants of the partition function and spin correlations, *Progress of Theoretical Physics* **56**, 1454 (1976).
- [S2] H. A. Kramers and G. H. Wannier, Statistics of the two-dimensional ferromagnet. part i, *Phys. Rev.* **60**, 252 (1941).
- [S3] Y. Liu, S. Lv, Y. Yang, and H. Zou, Signatures of quantum criticality in the complex inverse temperature plane, *Chinese Physics Letters* **40**, 050502 (2023).
- [S4] Z. Y. Xie, J. Chen, M. P. Qin, J. W. Zhu, L. P. Yang, and T. Xiang, Coarse-graining renormalization by higher-order singular value decomposition, *Phys. Rev. B* **86**, 045139 (2012).
- [S5] A. Denbleyker, Y. Liu, Y. Meurice, M. P. Qin, T. Xiang, Z. Y. Xie, J. F. Yu, and H. Zou, Controlling sign problems in spin models using tensor renormalization, *Phys. Rev. D* **89**, 016008 (2014).
- [S6] L. Zhang, Universal thermodynamic signature of self-dual quantum critical points, *Phys. Rev. Lett.* **123**, 230601 (2019).
- [S7] L. Zhang and C. Ding, Finite-size scaling theory at a self-dual quantum critical point, *Chinese Physics Letters* **40**, 010501 (2023).